October 1991

Important Considerations in Force Control With Applications to Multi-Arm Manipulation

Eric Paljug
University of Pennsylvania

Thomas G. Sugar
University of Pennsylvania

R. Vijay Kumar
University of Pennsylvania, kumar@grasp.upenn.edu

Xiaoping Yun
University of Pennsylvania

University of Pennsylvania Department of Computer and Information Science Technical Report No. MS-CIS-91-88.

Important Considerations in Force Control With Applications to Multi-Arm Manipulation

Abstract

This paper addresses force control in overconstrained dynamic systems with special emphasis on robot control and multiarm coordination. Previous approaches to force control are studied and many of these are shown to be unsuitable for *dynamic* force control. Practical and theoretical considerations for designing force control algorithms are discussed. Experimental and simulation results that validate the theoretical findings are presented for a single-degree-of-freedom pneumatic force controller. Finally the theoretical development of a two-arm manipulation system with an *extended statespace* formulation and a computer simulation of the system are presented to illustrate the application of the basic ideas to a more complicated system.

Comments

University of Pennsylvania Department of Computer and Information Science Technical Report No. MS-CIS-91-88.

Important Considerations In Force With Applications To Multi-Arm Manipulation

MS-CIS-91-88
GRASP LAB 287

Eric Paljug
Tom Sugar
Vijay Kumar
Xiaoping Yun

Department of Computer and Information Science
School of Engineering and Applied Science
University of Pennsylvania
Philadelphia, PA 19104-6389

October 1991

Submitted to the 1992 Conference On *Robotics and Automation*

Submitted to the 1992 IEEE Conference on Robotics and Automation.

Important Considerations in Force Control with Applications to Multi-Arm Manipulation

Eric Paljug, Tom Sugar, Vijay Kumar, and Xiaoping Yun

GRASP Laboratory
University of Pennsylvania
3401 Walnut Street, Room 301C
Philadelphia, PA 19104-6228

Abstract

This paper addresses force control in overconstrained dynamic systems with special emphasis on robot control and multiarm coordination. Previous approaches to force control are studied and many of these are shown to be unsuitable for *dynamic* force control. Practical and theoretical considerations for designing force control algorithms are discussed. Experimental and simulation results that validate the theoretical findings are presented for a single-degree-of-freedom pneumatic force controller. Finally the theoretical development of a two-arm manipulation system with an *extended state-space* formulation and a computer simulation of the system are presented to illustrate the application of the basic ideas to a more complicated system.

1 Introduction

1.1 Background

Force control is essential for the coordination of multiple actuators in an overconstrained robot system. Examples of such systems include a single robot interacting with the environment, multiple cooperating robots, and complex robot systems such as multifingered hands or walking vehicles. Although the basic idea of force control has been well-known for over a decade [20, 7], there are still some problems which are not clearly understood. Some of the limitations of force control are due to the lack of good actuators and sensors. In addition, there are several fundamental problems with the formulation and the implementation of force control algorithms. In this paper, we present theoretical and experimental results that provide an insight into these problems, and discuss applications to multiarm control.

1.2 Models for Force Control

Traditionally, models for robot dynamics have been derived from principles of rigid body dynamics. As a result, the force control problem has not been formulated as a dynamic control problem. When rigid body models are employed for the robot along with ideal actuator models, the actuator inputs are related to the positions through a second order differential equation. However, the output forces are algebraically related to the actuator forces (inputs) and therefore the formulation is devoid of dynamics. In other words, there is a lack of causality in the relationship between the output forces and the inputs. At best the actuators can *compensate* for forces in a *static manner*, but they cannot *dynamically* control the forces. In fact, theories for compliance (or stiffness) control [9, 21, 25, 30], operational space control [11], hybrid control [24] and their extensions to systems with closed chains [27, 31, 33] have the same limitations. In the past these theories proved to be adequate because the focus was on performing complex tasks in a quasi-static framework as opposed to dynamic control [26, 32, 10, 16], but dynamic control is not possible with this approach.

While rigid body models are justified when robots are position controlled, interactions with dynamic environments cannot be controlled with control laws derived from such models. This difficulty with rigid body models is identified in the work in References [17, 18], where the dynamic system is modeled by a singular system of differential equations and shown to exhibit impulsive behavior even with finite, well-behaved initial conditions. The basic idea is also recognized by Hogan and Colgate [2, 6]. They suggest that an impedance model for the contact be used for control system design. Seering and Eppinger in a series of papers [3, 5, 4] study problems that arise due to the noncolocation of sensors and actuators in force control schemes. In particular, they also consider dynamic models for the actuator, sensor and the environment.

This paper is closely related to previous work by the authors. For example, force control with unilateral constraints in studied in [34] and the application to multiple arm systems is described in [14]. The extension to nonholonomic systems is presented in [36]. The work described here focuses on a more fundamental problem: the dynamic control of forces in an overconstrained system.

1.3 Organization

In this paper, we study previous approaches to force control for constrained robot systems. We describe potential problems with these schemes, and point out theoretical and practical considerations that are important for the design of force control algorithms. Since most robotic controllers are implemented with a digital computer, we incorporate the effects of discretization into our analysis. The basic ideas are demonstrated with an experimental test-bed that is built with conventional (and inexpensive) actuators and sensors. We present design guidelines for force control schemes that are also applicable to stiffness control, hybrid control and simultaneous force-position control algorithms. Finally we show how these ideas can be implemented in the more complicated setting of multiarm control.

The paper is organized as follows: Section 2 discusses the conventional approaches to force control which relies on rigid body dynamic models. We show that an integrating compensator is absolutely essential in cases where the actuator dynamics are much faster than those of the controller. It is shown that since the integrating compensation is implemented by a digital controller, the method of discretization effects the resulting system dynamics. Section 3 develops a strategy for the opposite case where the actuator dynamics are much slower than the controller dynamics. It is clear that the actuator dynamics must be considered in the design of such controllers. Then, in Section 4, simulation and experimental data is presented to support the theoretical results of the previous sections. The basic ideas in this paper are applied to multiple arm manipulation in Section 5. Finally, the main points of this paper are summarized in Section 6.

2 Conventional Approaches to Force Control

Consider the force control problem of a robot system with n degrees of freedom. If I is the $n \times n$ inertia matrix, J is the Jacobian and τ is the vector of actuator forces/torques, then the dynamic equations of motion can be written as:

$$I(\theta)\ddot{\theta} + C(\theta, \dot{\theta}) + J^T F = \tau \tag{1}$$

where C is a nonlinear function of positions and velocities. This equation is of the form:

$$f(\theta, \dot{\theta}, \ddot{\theta}) + J^T F = \tau \tag{2}$$

If we decompose the input τ into τ_m and τ_f such that

$$f(\theta, \dot{\theta}, \ddot{\theta}) = \tau_m \tag{3}$$

$$J^T F = \tau_f \tag{4}$$

it is possible to design a position control scheme with τ_m as the input and a force control scheme with τ_f as the input. This is, in essence, the model used in numerous papers (see for example, [15, 1, 12, 23, 24, 27, 37]). However it is quite obvious that (4) is algebraic in nature and is devoid of dynamics. At best, the actuators can *compensate* for external forces in a *static* manner.

Alternatively, in the state-space formulation, Equation 1 is of the form:

$$\begin{aligned} \dot{x} &= A(x)\,x + B(x)\,u \\ -1y &= C(x)\,x + D(x)\,u \end{aligned}$$

where x, y, and u are the state, output and input, respectively. (For example, $x = [\theta^T, ; \dot{\theta}^T]^T$, $y = F$ and $u = \tau$.) Note that here $D(x)$ is *nonzero* unlike conventional trajectory control problems.

2.1 A Simplified Force Control Problem

In the rest of the paper, we deal with a simplified force control problem in one dimension. Consider the equation:

$$y(t) = D\,u(t) \tag{5}$$

where D is a constant relating input force/torque u to output force y. Throughout this paper it is assumed that $D > 0$. This equation, like Equation 4, does not include any actuator dynamics and employs a rigid body contact model.

The dynamics of the actuator and the dynamics of contact interaction can also be explicitly modeled. For example, if these can be adequately represented by a second order system (natural frequency ω_a, damping ratio ζ_a and steady-state gain D), the output force is related to the input by the equation:

$$\frac{1}{\omega_a^2}\frac{d^2y}{dt^2} + \frac{2\zeta_a}{\omega_a}\frac{dy}{dt} + y = Du \tag{6}$$

or using Laplace transforms:

$$\frac{Y(s)}{U(s)} = \frac{D}{\frac{s^2}{\omega_a^2} + \frac{2\zeta_a s}{\omega_a} + 1} \tag{7}$$

The simplified model in Equation 5 is a valid approximation to the system in Equation 6 provided ω_a is very large. If the desired force y_d is given, the input u can be calculated as:

$$u(t) = \frac{y_d(t)}{\hat{D}} \tag{8}$$

where $\hat{D}$ is the estimated (modeled) value of D. The relation of the output to the desired output is given as:

$$y(t) = \frac{D}{\hat{D}}\,y_d(t) \tag{9}$$

Clearly, if $\hat{D} = D$, nothing further needs to be done. But, if there is a discrepancy, then there is always a finite error. (This discrepancy could be attributed to calibration errors, inaccuracies in modeling, parameter drift, noise, etc.) Thus there is a need for a feedback control scheme and this is the subject of the next several subsections.

2.2 Proportional Control

The simplest feedback law is obtained as follows:

$$u(t) = \frac{y_d(t)}{\tilde{D}} + K_p(y_d(t) - y(t)) \tag{10}$$

where K_p is the proportional control gain. Substitution into Equation 9 yields

$$y(t) = \frac{DK_p + \frac{D}{\tilde{D}}}{DK_p + 1} y_d(t) \tag{11}$$

If there is no noise, for large K_p, the error is close to zero and it is easy to conclude that forces can be controlled by proportional control.

This analysis is not quite complete because the control law given by Equation 10 with the model of Equation 9 leads to a system which is static and therefore characterized by algebraic equations. It is meaningless to talk about the stability or convergence of such schemes. The potential practical problems with this scheme are evident when we try to implement such a scheme with computer control. (The effects of discretization are discussed in Section 2.4 and it is shown that the proportional gain is limited to $\frac{1}{D}$ for stability.)

2.3 Proportional plus Integral Control

In the above analysis, since the only possible problem with proportional control is the presence of a steady-state error (there is no transient in a static system), it is natural to add the integral of the error in the feedback loop. This has been the basic approach in [1, 12, 37], although these papers did not clearly justify the need for the integral component.

This elimination of steady state error is one advantage. The second advantage of employing integral control is that it does introduce causality into the system [29]. The control law

$$u(t) = \frac{y_d(t)}{\tilde{D}} + K_I \int (y_d(t) - y(t))\, dt + K_p(y_d(t) - y(t)) \tag{12}$$

leads to the following input-output equation in s-domain:

$$Y(s) = Y_d(s) \left(\frac{s\left(\frac{1 + K_p\tilde{D}}{K_I\tilde{D}}\right) + 1}{s\left(\frac{1 + K_pD}{K_ID}\right) + 1} \right) \tag{13}$$

The need for using dynamic state feedback for force control has been formally justified in an earlier paper [35, 14], and the use of such a scheme has been demonstrated for multiarm control in [34, 14, 19]. In fact, it is shown in these papers that a pure integral control scheme ($K_p = 0$, $K_I \neq 0$) ensures stability, and simulations are presented to illustrate the robustness of the approach.

2.4 Discrete Control Laws

While continuous system theory explains the effect of proportional and integral gains, it is beneficial to investigate the effects of discretization which are inevitable in digital controllers. We assume a digital control system in which the sampling interval is T_s and the sampling frequency is ω_s. Of course, a rigid body model is justified only if the frequencies of operation are much smaller than the natural (characteristic) frequency of the physical system ω_a. Since the frequency of operation is limited by the Nyquist frequency, it is safe to state that a rigid body approximation can be employed whenever $\omega_s \ll \omega_a$. In fact, the exact requirement is that the delay τ_d between the controller's output (commanded voltage) and input (measured error signal) must be greater than the settling time of the actuator due to a step input. In what follows we consider the effects of discretization on static and dynamic feedback schemes.

In the case of integral control, since the controller introduces causality into an otherwise static system, the method of discretization is particularly important. For example, consider the systems obtained by using two candidate difference rules — the backward difference rule and the trapezoidal difference rule:

$$s = \frac{z\ -\ 1}{T_s z}; \quad s = \frac{2}{T_s}\left(\frac{z\ -\ 1}{z\ +\ 1}\right) \tag{14}$$

where z^{-1} is the discrete delay operator and T_s is the controller sampling period.

The discrete control law must be causal, which restricts the calculation of u to be a function of the physical system data from the *previous* sample periods. However, this restriction does not apply to the desired variable y_d because it may be known *a priori*. Thus, the discrete control law is a function of the form:

$$u(k)\ =\ \mathcal{F}(\, y(k-i),\, y_d(k),\, y_d(k \pm i)\,) \qquad i \geq 1 \tag{15}$$

The substitution of the backward and trapezoidal difference rules into Equation 12 while satisfying Equation 15 yields the discrete control laws:

$$u_{back}(z)\ =\ \frac{y_d(z)}{\tilde{D}}\ +\ K_I\left(\frac{T}{z\ -\ 1}\right)(y_d(z) - y(z))\ +\ K_p\left(z^{-1}\right)(y_d(z) - y(z)) \tag{16}$$

$$u_{trap}(z)\ =\ \frac{y_d(z)}{\tilde{D}} + K_I\frac{T}{2}\left(\frac{z+1}{z-1}\right)\left(z^{-1}\right)(y_d(z) - y(z)) + K_p\left(z^{-1}\right)(y_d(z) - y(z)) \tag{17}$$

where Equations 16 and 17 correspond to the use of the backward and trapezoidal difference rules, respectively.

These control laws are then applied to the discrete form of the continuous system model (Equation 5) given as:

$$y(z)\ =\ D\, u(z) \tag{18}$$

which results in the discrete transfer functions:

$$y(z)\ =\ y_d(z)\left(\frac{D}{\tilde{D}}\right)\left(\frac{z^2\ +\ (K_I T\,\tilde{D} + K_p\tilde{D} - 1)z\ -\ K_p\tilde{D}}{z^2\ +\ (K_I T\,D + K_p D - 1)z\ -\ K_p D}\right) \tag{19}$$

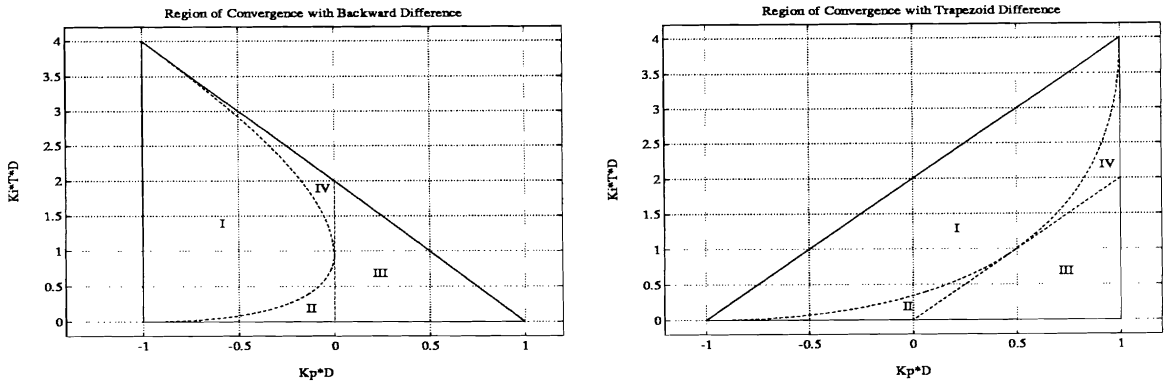

(a) (b)

Figure 1: Region of Convergence for (a) Backward and (b) Trapezoidal Difference Systems

$$y(z) \quad = \quad y_d(z)\left(\frac{D}{\tilde{D}}\right)\left(\frac{z^2 + (\frac{K_I T\tilde{D}}{2} + K_p\tilde{D} - 1)z + \frac{K_I T\tilde{D}}{2} - K_p\tilde{D}}{z^2 + (\frac{K_I T D}{2} + K_p D - 1)z + \frac{K_I T D}{2} - K_p D}\right) \tag{20}$$

where Equation 19 is derived with the backward rule and Equation 20 uses the trapezoidal rule.

The above systems are stable when the poles of the Equations 19 and 20 are within the unit circle of the Z-plane. This stability condition bounds the values of K_I and K_p, and the boundaries vary significantly depending on the difference rule employed. For the backward difference rule, the stability bounds are

$$\|K_p D\| < 1\ , \quad \|\frac{K_I T\, D}{2} + K_p D\| < 1\ , \quad K_I > 0 \tag{21}$$

and the bounds for the trapezoidal difference rule are

$$\|K_p D\| < 1\ , \quad \|\frac{K_I T\, D}{2} - K_p D\| < 1\ , \quad K_I > 0 \tag{22}$$

These boundaries and the "stable" regions are depicted on the plane of $K_p D$ versus $K_I T\, D$ in Figure 1.

The range of allowable gains shown in Figure 1 can be subdivided into four regions. These different regions correspond to different locations of the poles within the unit circle. Region I contains the underdamped poles, and Region II contains the overdamped poles. The remaining regions have one (Region III) or both (Region IV) poles on the negative real axis of the Z-plane. A pole located on this part of the Z-plane corresponds to a pole in the s-plane of the form $s = a \pm i\omega_s/2$ where $-\infty < a \leq 0$ and ω_s is the sampling frequency. The point where all four internal regions intersect corresponds to two poles at $z = 0$ in the Z-plane.

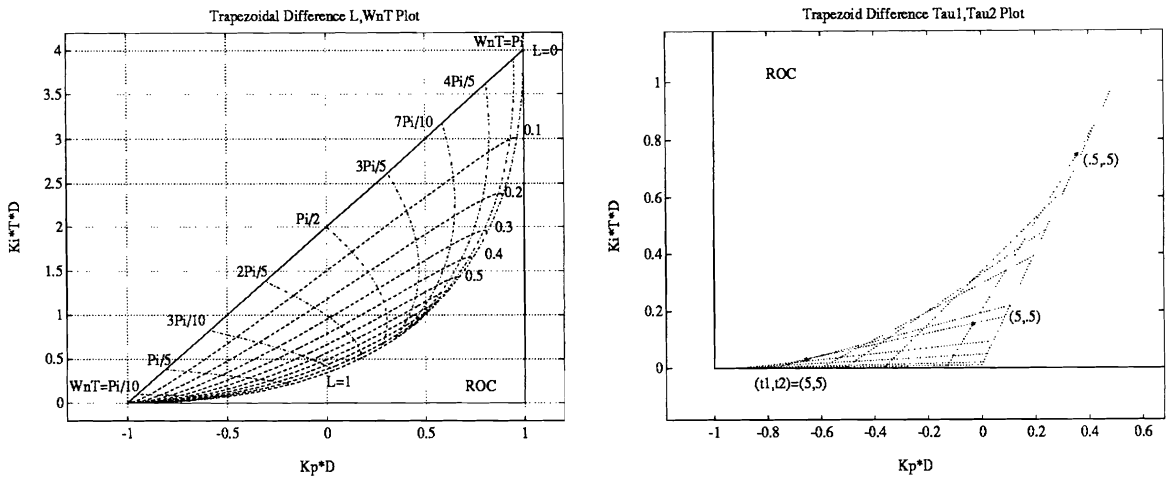

(a) (b)

Figure 2: Choosing Gains from System Specifications for Trapezoid Difference Implementation

It is interesting to note that these figures show that the system is stable even for negative values of K_p. In fact, if $K_I = 0$, then a stable response requires $\|K_p\| < 1$ but a standard first order exponentially decaying response requires negative K_p (resulting in a single pole on the positive real axis of the Z-plane). When $K_I T\, D > 0$ and the choice of K_I and K_p fall within the stability boundries, the system exhibits a variety of second order responses, even if K_p is zero. The widest assortment of responses is obtained with combinations of non-zero K_p and K_I.

Figure 2 is a magnified view of Regions I and II for the trapezoidal case and provides a guideline in designing the response of system. The values of K_I and K_p can be estimated from Figure 2.a for a desired underdamped system response characterized by a damping ratio L (ζ) and a natural frequency Wn (ω_n). Figure 2.b can be used to estimate K_I and K_p for an overdamped system response characterized by the time constants Tau1 and Tau2 (τ_1 and τ_2). It is important to note that each axis in Figure 2 is scaled with respect to the system variable D. Since it is assumed that this value is not exactly known, it's estimate $\tilde{D}$ can be used for selecting gains for control system design. But it should be remembered that the resulting values for K_I and K_p will correspondingly only be *estimates* of gains for the desired response parameters.

The plots in Figure 3 show the step response for the Trapezoidal difference rule implementation. A representative graph of each region is shown for two different $\tilde{D}/D$ ratios (.7 and 1.3). In each case, since $K_I \neq 0$, the system exhibits a steady state error of zero for a unit step input.

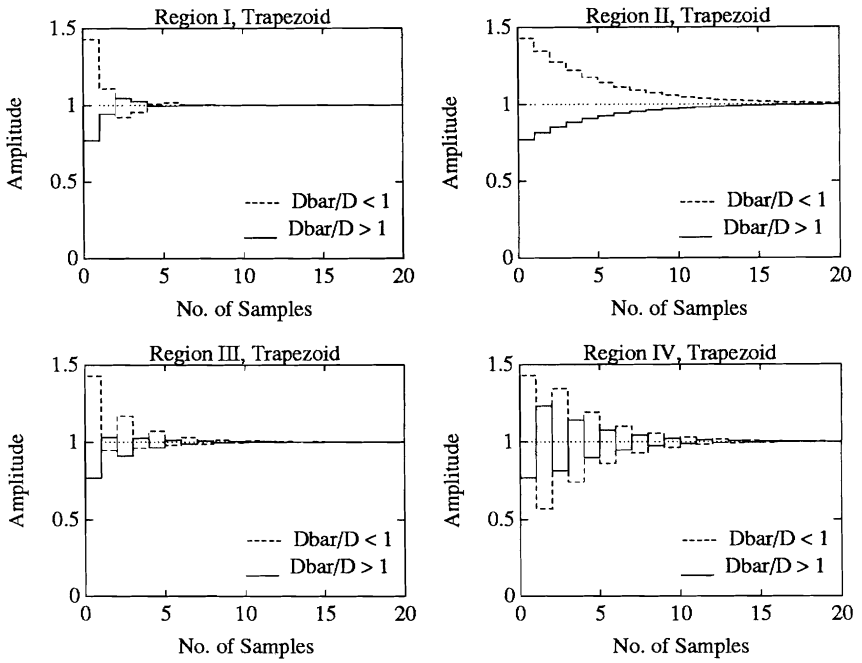

Figure 3: Input step response with the trapezoidal difference rule.

3 Force Control with a Causal Model

When the $\omega_s \ll \omega_a$ assumption is not valid, there is no justification for using the acausal model in Equation 1. It is essential to incorporate a model of the actuator dynamics, such as the one in Equation 7, into the control system design. It is clear that the input is now causally related to the output. We examine the implications and the effect of errors caused by approximate models using the example of a single degree-of-freedom pneumatic force controller. We later substantiate the theoretical analysis with simulations and experimental data.

3.1 Example of a pneumatic force controller

We consider a double-ended, linear, pneumatic actuator with a force sensor. The actuator consists of two single-ended, graphite-glass cylinders (without seals). The actuator is driven by a flow-control valve and the differential pressure in the cylinders is fedback through an analog proportional loop in order to enhance the force controllability. The force control law is implemented on a PC-AT compatible computer. The block diagram for the control scheme is presented in Figure 4. A detailed description of the experimental test-bed is presented in the appendix.

Analytical modeling of pneumatic systems is quite difficult. The primary reasons are the compressibility of air, variation of the system parameters with temperature which increases with time, and nonlinearities due to friction at the seals [22, 28]. (The experimental test-bed uses graphite-glass cylinders which does minimize the effects of friction.) Instead, we

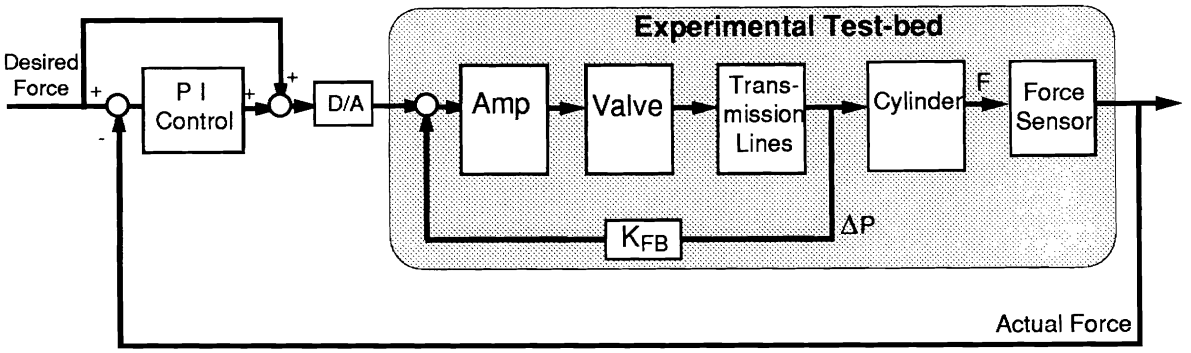

Figure 4: Block diagram of pneumatic control system

adopt an experimental approach in which we use standard system identification techniques to develop an experimental model.

The open-loop model for the valve, actuator, inertia, force sensor and the contact is developed through sinusoidal testing. The input to the valve is a swept sine signal while the output is the voltage recorded at the force sensor. A Hewlett-Packard dynamic signal analyzer facilitated this process. The open-loop model does have an inner feedback loop that is accomplished by the analog feedback of the cylinder pressure as shown in Figure 4. The feedback gain K_{fb} can be varied between zero and one. The frequency response obtained for this system is shown in Figure 5 for two different (analog) feedback gains. (Broadly speaking, the larger the feedback gain, the better the performance of the closed loop force controller). In each case, models for the system were obtained through curve fitting. These transfer functions are:

1. $K_{fb} = 0.5$

$$\frac{Y}{U}(s) = \frac{88380(s+37)}{(s+5.6)(s+32)(s^2+29s+5485)} \tag{23}$$

2. $K_{fb} = 1.0$

$$\frac{Y}{U}(s) = \frac{131300(s+48)}{(s+11)(s+62)(s^2+30s+5283)} \tag{24}$$

Note that these transfer functions are obtained with small signal testing so that the linear model assumption is valid. Approximate analytical models and experimental validation is discussed in [28]. We also note that while a higher order systems may produce an arguably better match when fitted to the actual system data, such a procedure does not completely eliminate modeling errors. Further, higher order fits also result in a more complex model which complicates controller design and simulation.

3.2 Control laws

Pursuing the example of the pneumatic force controller further, we can see both models of Equation 23 and 24 result in causal (non-algebraic) relation between the input and the

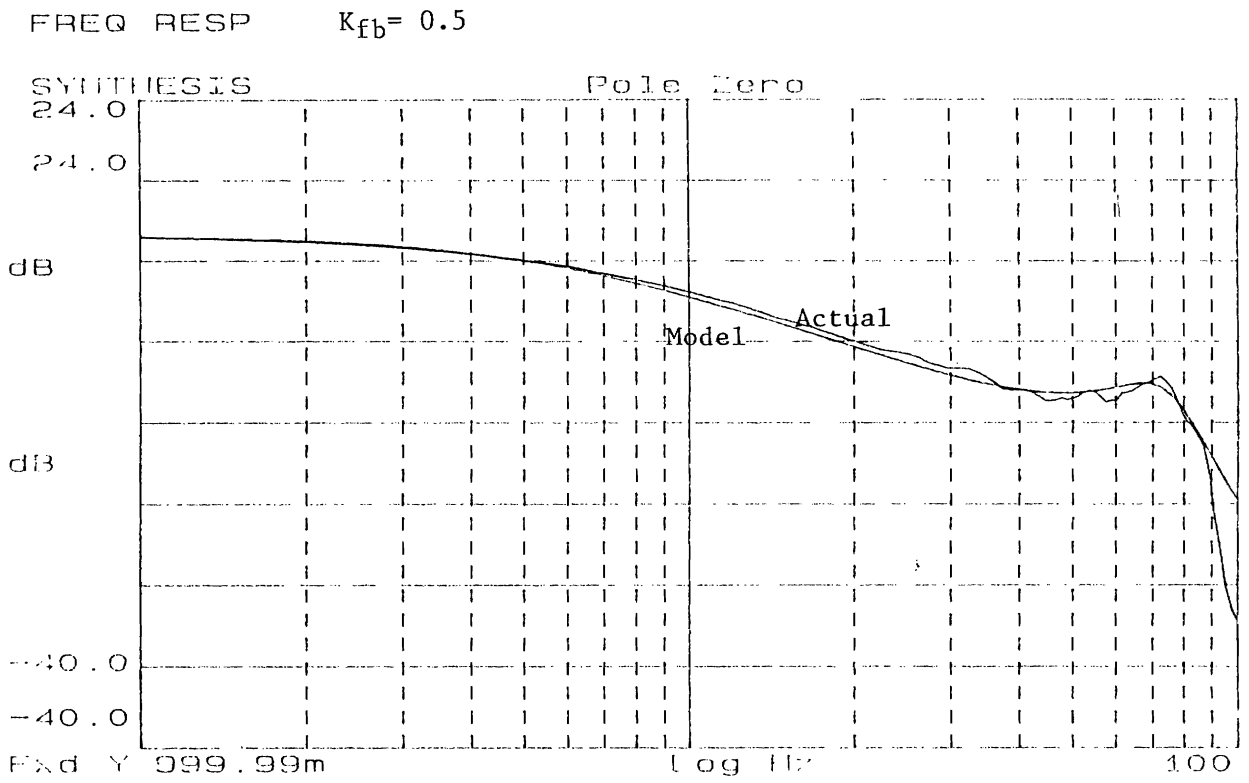

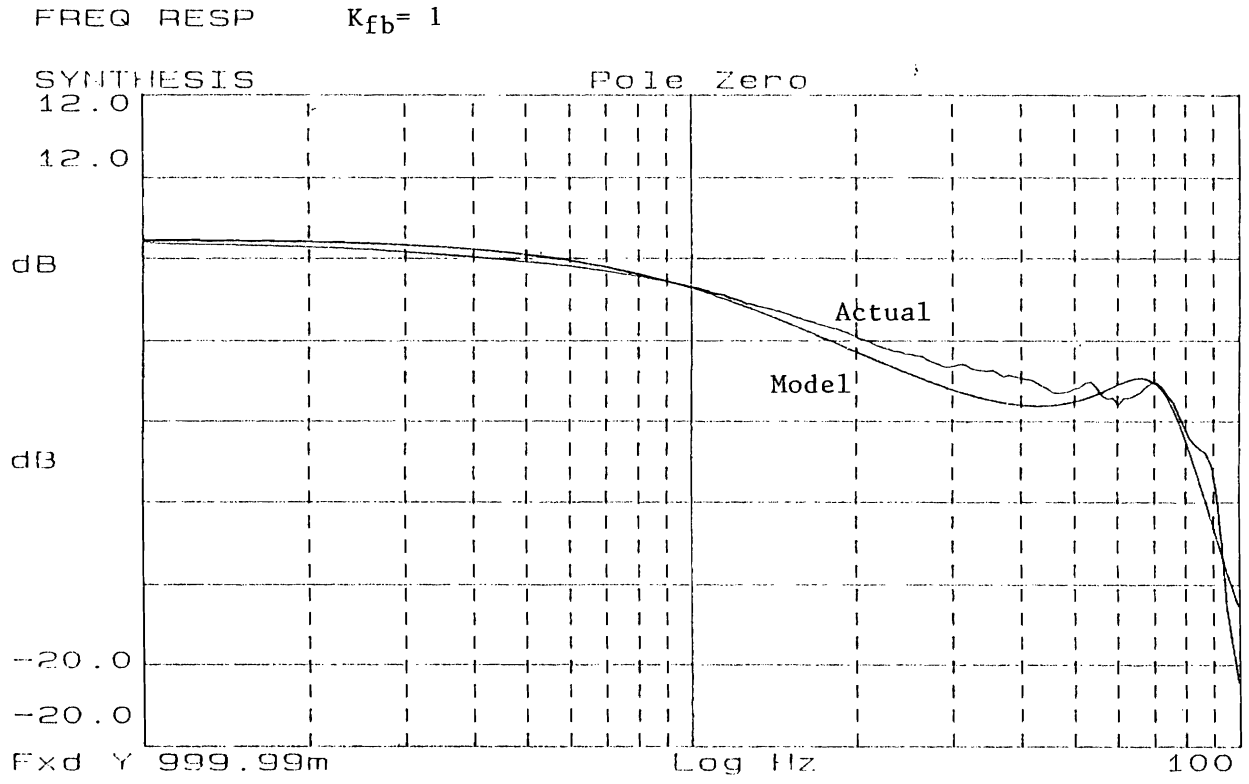

Figure 5: Frequency response of the pneumatic system for K_{fb} equal to 0.5 and 1.0.

output. A variety of feedback control algorithms can be designed for such a system. We prefer the simple proportional and proportional plus integral control laws for the following reasons. First, an accurate experimental model is not likely to be available. And sophisticated model-based controllers such as those based on inverse dynamics schemes are not necessarily superior when the model is not completely correct. Second, the main objective of this paper is to investigate the possible perils with rigid-body, acausal assumptions and the simple control laws that are used with such models. Finally, even with sophisticated models, in many cases, such simple controllers prove to be satisfactory.

4 Experiments with Force Control

In this section, we examine the performance of different control laws. We present simulation results obtained with the analytical models in Equations 23 and 24 and experimental results obtained from the test-bed. The trapezoidal difference rule is implemented in the digital control law of both the experimental test-bed and the simulation. Two cases are investigated:

1. Case 1: The sampling frequency is well below the characteristic frequency of the system ($\omega_s \ll \omega_a$)
2. Case 2: The system dynamics is much slower than the sampling frequency ($\omega_a \ll \omega_s$)

In each case, the results are compared and discussed with relation to the analysis in the previous sections. (Note the experiments were conducted with unit steps between 1 and 2 pounds while the simulation illustrates responses for the unit step between 0 and 1 pound.) The simulation was implemented with the MATLAB software package.

4.1 Case 1

In this case, the physical system reacts much quicker than the digital controller. Here it is meaningful to apply the analysis of Section 2 where the input torque and output force are algebraically related. This case is realized by restricting the digital controller to a sampling rate of 3 Hz, well below the bandwidth of the actuator system with $K_{fb} = 1$ (approximately 15 Hz.).

In the following figures, the simulation and experimental data are organized side by side for the same tests. The simulation is based on the actuator model derived from experiments as shown in Figure 24. Each plot depicts the actual force (in lbs.) measured by the sensor as a solid line, the desired force signal (in lbs.) as a dashed line, and the output signal of the digital controller (in volts) as a dotted line. Figure 6 shows the step response with $K_I = 0$ and $K_p\tilde{D} = 0.4$. Note in this case that the experimental data and the simulation both show (as predicted by the theory) a steady state error due to $\frac{\tilde{D}}{D} \neq 1$. When K_I is used, the steady state error is eliminated, as expected. Figures 7 and 8 show the step response for Regions I and II. The underdamped response (Region I) is obtained with $K_I T\,\tilde{D} = 2.2$ and $K_p\tilde{D} = .6$ while the overdamped response (Region II) has gains $K_I T\,\tilde{D} = 0.2$ and $K_p\tilde{D} = -0.1$. A comparison of these plots with Figure 3 shows that they are also in accordance with the theoretical analysis of Section 2.

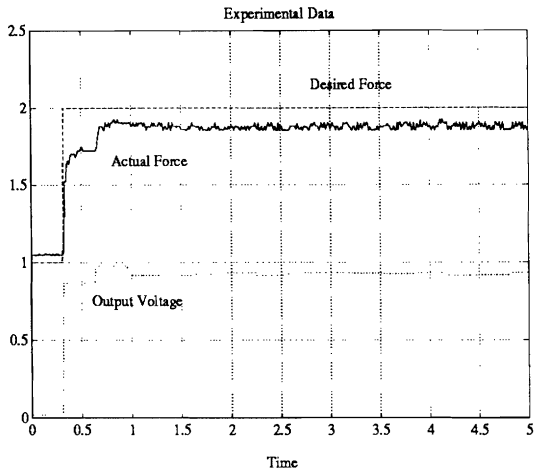

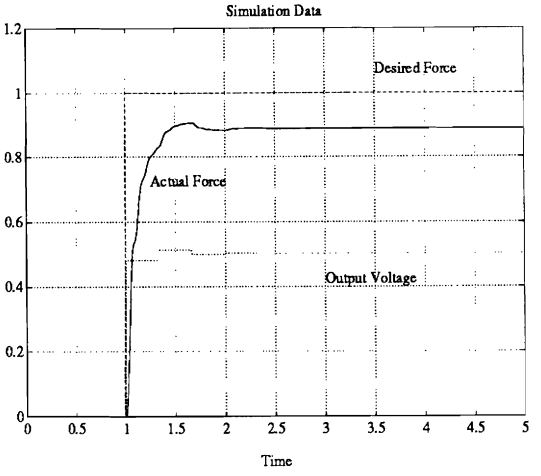

(a) (b)

Figure 6: Case 1: Proportional control with $K_I T\,\tilde{D} = 0$, $K_p\tilde{D} = 0.4$

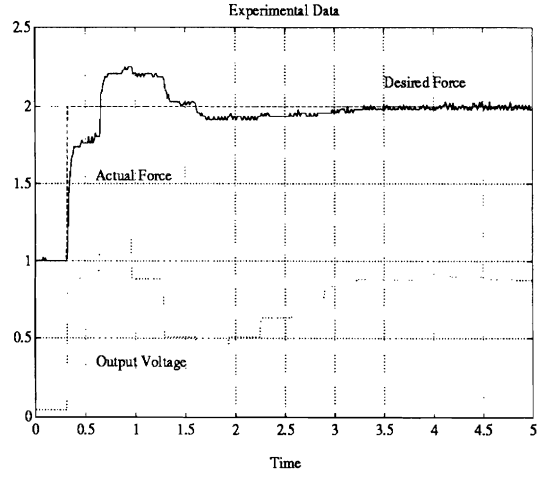

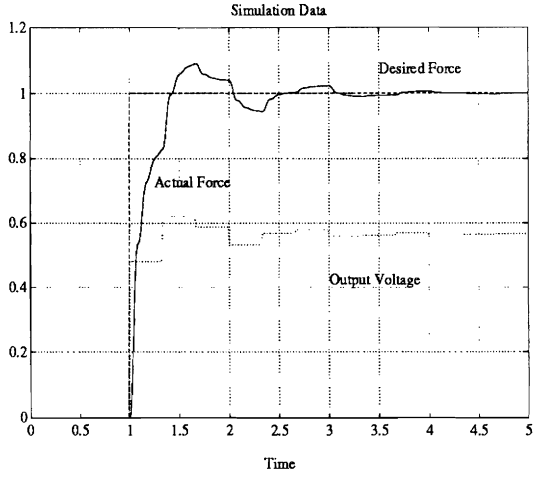

(a) (b)

Figure 7: Case 1: Underdamped response with $K_I T\,\tilde{D} = 2.2$, $K_p\tilde{D} = 0.6$

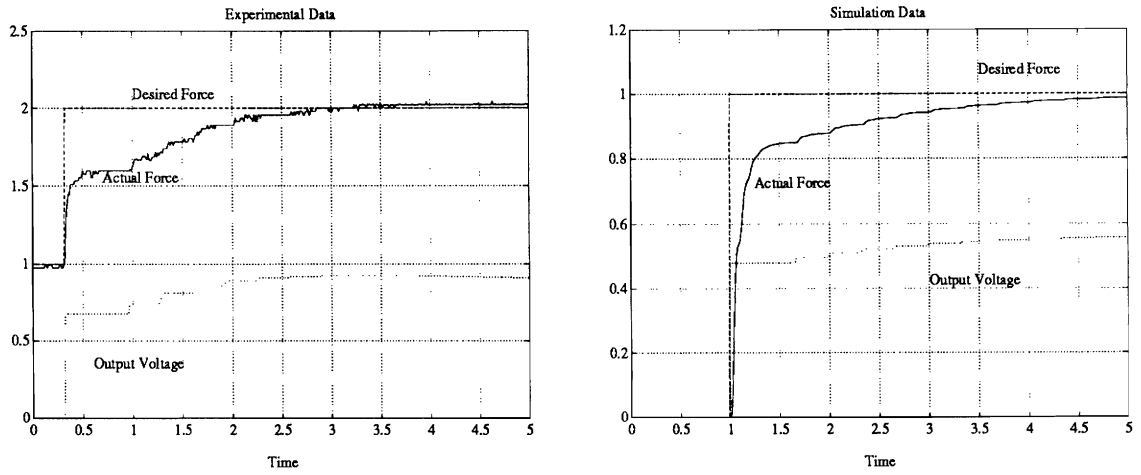

(a) (b)

Figure 8: Case 1: Overdamped response with $K_I T \tilde{D} = 0.2$, $K_p \tilde{D} = -0.1$

4.2 Case 2

This section presents the case in which the sampling frequency of the digital controller is much larger that the bandwidth of the physical system. To realize this large difference between the sampling frequency and the actuator's bandwidth, the analog feedback of the physical system (K_{fb}) is set to 0.5 and the digital controller of the both the experimental test-bed and the simulator samples at 150 Hz. The simulation incorporates the actuator model that is derived from the measured frequency response (Equation 23).

Again, simulation and experimental data for the same tests are presented in each figure and the solid line is the actual force, the dashed line is the desired force, and the dotted line is the digital controller output. The first plot (Figure 9) shows the response of the system with only proportional compensation. There is a non-zero steady state error. As K_p is increased, the physical system becomes unstable.

Figure 10 depicts a trial with integral and proportional compensation ($K_p = 0.8$ and $K_I = 8$). The results show a response in which the error converges toward zero. The type of behavior exhibited in these plots does not reflect the analysis of Section 2 because the basis of that analysis is an instantaneous model and in this case the physical system certainly has a causal response.

The discrepancies between the experimental and simulated data reflect the difficulties in finding simple and accurate models for the actuator. In particular, the modeling errors in the high frequency range (above 50 Hz.) are significant. The main sources of error are thought to be the friction in the servovalve and the actuator cylinder, the compressibility of air and the change in the thermodynamic properties caused by the increase in temperature over time.

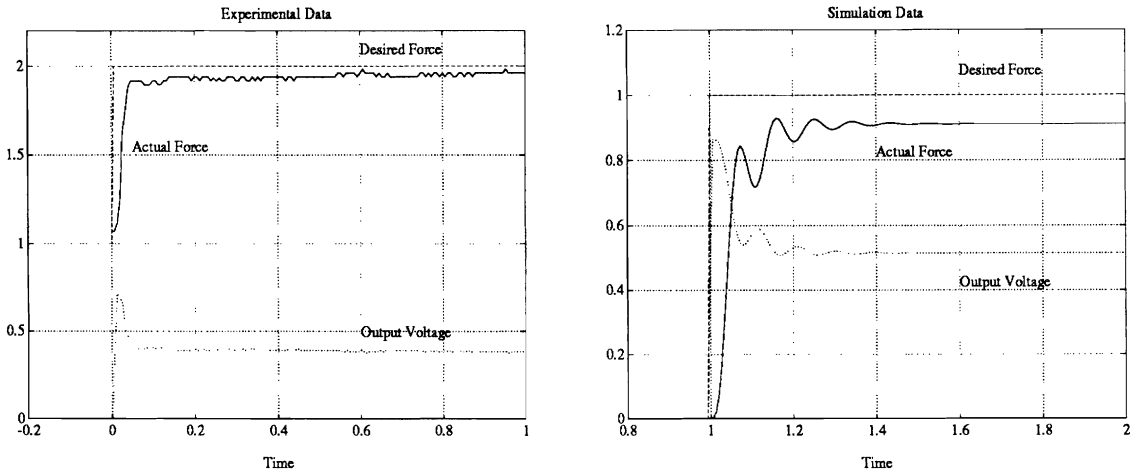

(a) (b)

Figure 9: Case 2: Proportional control with $K_I = 0$, $K_p = 0.8$

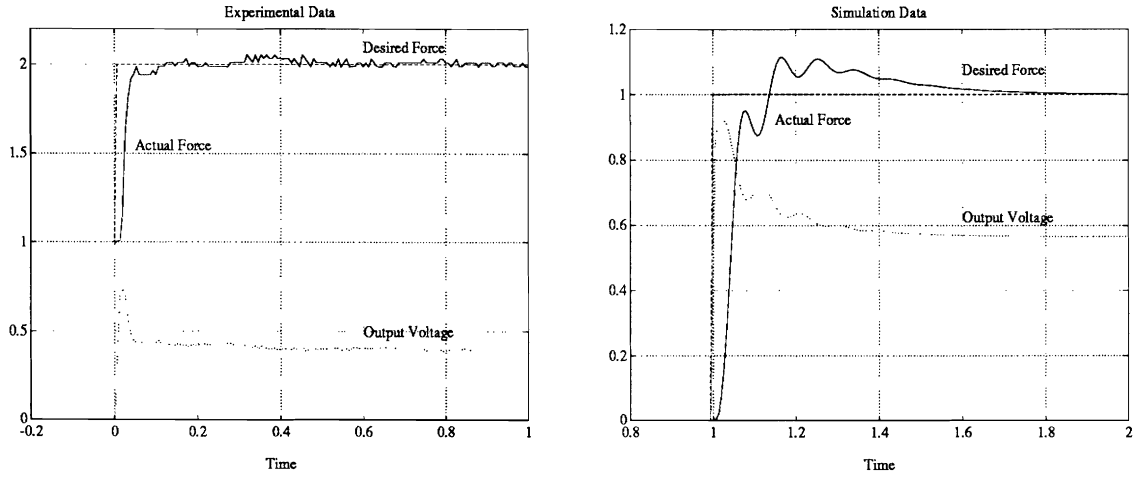

(a) (b)

Figure 10: Case 2: Integral and Proportional control with $K_I = 8.0$, $K_p = 0.8$

4.3 Summary

We have shown through computer simulation and experimentation that

- The approach to force control with an acausal model is fraught with perils. At the very least it is necessary to include an integrator in the control law. Further, the effect of discretization must be thoroughly investigated. The dynamics of the system is a strong function of the implementation of the control law.
- The design of control laws (and the selection of gains) based on a rigid body model and an algebraic actuator model (as presented in Section 2.1) is only valid when $\omega_s \ll \omega_a$.
- In the case when $\omega_a \ll \omega_s$, the model is causal. Here force control schemes can be designed using the conventional approach. Obtaining actuator models can be difficult. However, with a knowledge of a characteristic frequency for the system, it is possible to select gains so that simple control laws yield the desired performance.

Although the system studied in this paper is a pneumatic system, the same basic principles apply to electrical and hydraulic actuators as well. In most conventional robot arms, DC servo motors are used as actuators. Typically they have a higher control bandwidth (under low loads) and with rigid effectors and environment, ω_a is very high. Thus most typical situations fall into the Case 1 category and the theoretical analysis in Section 2 is directly applicable.

5 Force Control in Multi-Arm Manipulation

5.1 Contact Forces

When multiple arms are employed to manipulate objects it is necessary to control not only the trajectory of the system but also the contact forces between each arm (or the effector of the arm) and the object. In the context of force control, it is necessary to control either the internal (interaction) forces [10, 26, 13] or the *critical contact forces* [14, 34].

The critical contact forces is merely a vector of minimum set-points for force components that are critical for prehension. For example, when manipulating an object with two rigid, convex surfaces as shown in Figure 11, we have two frictional point contacts, with contact forces F_1 and F_2. The critical contact force is given by:

$$\begin{aligned} F_c &= \min\{e_{12} \cdot F_1, -e_{12} \cdot F_2\} \\ &= \frac{e_{12} \cdot F_1 - e_{12} \cdot F_2 - \mid e_{12} \cdot F_1 + e_{12} \cdot F_2 \mid}{2} \end{aligned}$$

where e_{12} is a unit vector along the line joining the two points of contact. Clearly, if a rolling contact is desired, then $F_{c,desired}$ is selected to have a sufficiently large value in order to prevent slip.

In general, the trajectory variables and the contact forces in the multi-arm robotic system (and this includes the critical contact forces) can be expressed in state space notation in the form:

$$\ddot{\zeta} = f(\zeta, \dot{\zeta}) + g(\zeta)\tau \tag{25}$$

$$\lambda = a(\zeta, \dot{\zeta}) + b(\zeta)\tau \tag{26}$$

where τ is the vector of actuator inputs, ζ is the vector of generalized coordinates, and λ is the vector of contact forces. Note the pathological situation due to the force (λ) being directly related to the actuator input (τ) through the function $b(\zeta)$.

The dynamic control of the force *extended state space formulation* [34, 14, 19]. In this approach, we expand the state to include the actuator torque (or, equivalently, we introduce an integrator on each input):

$$x = [x_1 \quad x_2 \quad x_3]^T = [\zeta \quad \dot{\zeta} \quad \tau]^T$$

Thus, the general form of Equation 25 and 26 under the new state x becomes:

$$\begin{aligned} \dot{x} &= \begin{bmatrix} \dot{x}_1 \\ \dot{x}_2 \\ \dot{x}_3 \end{bmatrix} = \begin{bmatrix} x_2 \\ f(x_1, x_2) + g(x_1)x_3 \\ 0 \end{bmatrix} + \begin{bmatrix} 0 \\ 0 \\ I \end{bmatrix} u \\ &= \xi(x) + \eta(x)u \end{aligned} \tag{27}$$

and the output equations have the form

$$y = \begin{bmatrix} y_1 \\ y_2 \end{bmatrix} = \begin{bmatrix} x_1 \\ E(x_1)^T \left(a(x_1, x_2) + b(x_1)x_3\right) \end{bmatrix} \tag{28}$$

where $E(x_1)$ is a projection matrix, and y is divided into its position components (y_1) and its force components (y_2). Now the forces are a function of the state x only and there is now a causal relationship between the input u and the force y_2.

In Section 2, we showed the importance of introducing dynamics into force control and how a variety of responses are obtainable by adjusting the gain on the integrating compensation. The above scheme accomplishes exactly this effect. In this particular formulation, we restrict ourselves to a pure integral control law, a control law which was shown to be stable in Section 2.

An example of a two arm robotic system is presented to clearly illustrate the control scheme. In this example, each robot is a three-link, serial, planar manipulator with revolute joints. The object is circular with its center of mass located at the center of the circle. (See Figure 11.) The two effectors are flat palmar surfaces. The robots make point contacts with the object and the control task is to manipulate the object while preventing separation or slipping at the contact points. This requires explicit control of the critical contact force as well as the position variables, which include the circle's position and the orientation of the robot contact surface. If we use the definition of the critical contact force as in Equation 25, the output variables for the controller are the trajectory of the object (x_o, y_o, ϕ_o), the orientation of the two palms, ϕ_1 and ϕ_2, and the force F_c. The control of the orientation variables will allow the system to perform controlled rolling of the contact points, which is useful in satisfying all the goals of the task.

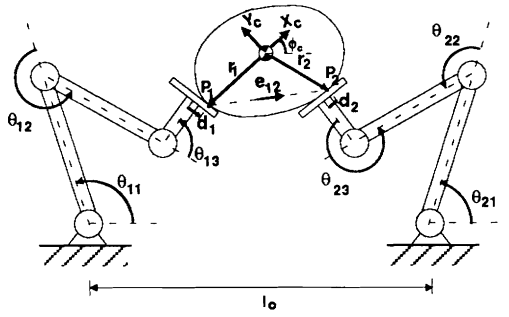

Figure 11: Two 3-R robot arms manipulating an object

5.2 Nonlinear Feedback

The controller design for the system given in Equation 27 and 28 is accomplished using a nonlinear feedback which linearizes and decouples the system [14]. The feedback has the form:

$$u = \alpha(x) + \beta(x)v \tag{29}$$

where $\alpha(x)$ and $\beta(x)$ are to be constructed based on the system model. Using differential geometric design techniques [8] for nonlinear systems, $\alpha(x)$ and $\beta(x)$ can be found by solving the following matrix equations [35]

$$\Phi(x)\alpha(x) = -\begin{bmatrix} L_\xi^3 y_1 \\ L_\xi y_2 \end{bmatrix} \; ; \quad \Phi(x)\beta(x) = I \tag{30}$$

where $\Phi(x)$ is the decoupling matrix of the system which is given by

$$\Phi(x) = \begin{bmatrix} L_\eta L_\xi^2 y_1 \\ L_\eta y_2 \end{bmatrix}$$

and $L_\nu y_i$ is the Lie derivative of y_i along the vector field ν. Application of the above feedback linearizes the system in a transformed state space z. The new state variable z, and x are related by [8]

$$z = [z_1 \quad z_2 \quad z_3 \quad z_4]^T = [y_1 \quad L_\xi y_1 \quad L_\xi^2 y_1 \quad y_2] \tag{31}$$

where $L_\xi y_i$ is the Lie derivative of y_i along the vector field ξ. The linearized system is characterized by

$$\begin{bmatrix} \dot{z}_1 \\ \dot{z}_2 \\ \dot{z}_3 \\ \dot{z}_4 \end{bmatrix} = \begin{bmatrix} 0 & I & 0 & 0 \\ 0 & 0 & I & 0 \\ 0 & 0 & 0 & 0 \\ 0 & 0 & 0 & 0 \end{bmatrix} \begin{bmatrix} z_1 \\ z_2 \\ z_3 \\ z_4 \end{bmatrix} + \begin{bmatrix} 0 & 0 \\ 0 & 0 \\ I & 0 \\ 0 & I \end{bmatrix} \begin{bmatrix} v_1 \\ v_2 \end{bmatrix} \tag{32}$$

and the output equation is given by

$$\begin{bmatrix} y_1 \\ y_2 \end{bmatrix} = \begin{bmatrix} I & 0 & 0 & 0 \\ 0 & 0 & 0 & I \end{bmatrix} \begin{bmatrix} z_1 \\ z_2 \\ z_3 \\ z_4 \end{bmatrix} \tag{33}$$

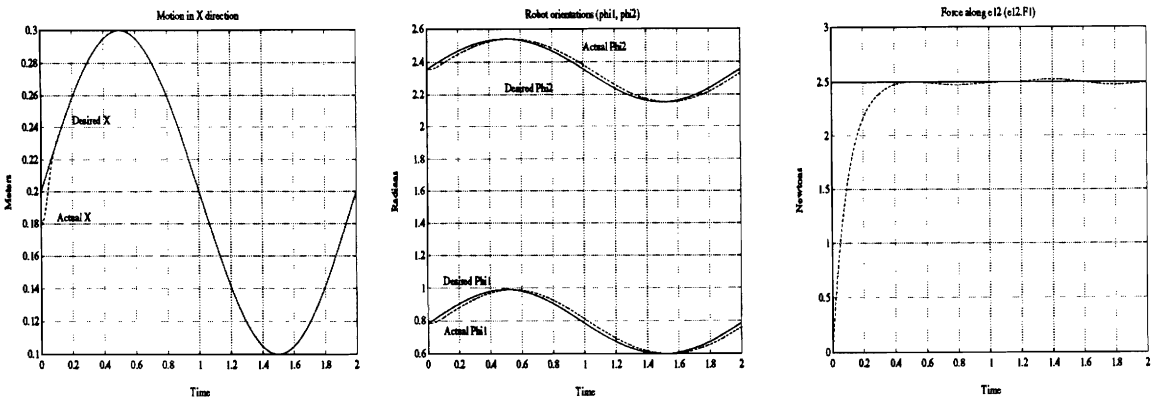

(a) (b) (c)

Figure 12: Simulation of two 3 DOF robots manipulation an object.

5.3 Simulation

We have developed a computer simulation of the planar system in Figure 11. In the simulation trial presented, the goal is to move the circular object sinusoidally along the x direction while maintaining constant y and the object orientation ϕ and at the same time controlling the critical contact force. The control of the critical contact force and object motion requires the orientation of the robots at the the contact points (ϕ_1, ϕ_2) to change (by rolling) if the force applied at each contact point is to stay centered within the contact friction cone (thus preventing contact slippage.) Figure 12 shows the actual and desired plots for the object's x position, and the robot orientations ϕ_1, ϕ_2 and $e_{12} \cdot F_1$. Note the dynamic response in the force graphs due to the introduction of the integrators. Because of this, the decoupled force control subsystem is of first order and this is evident from the response. (The force signal exhibits small perturbations that are attributable to the gravity being unmodelled within the controller.)

5.4 Summary

The development in this section illustrates the formulation of the force control problem in systems where the position and force control problem must be simultaneously addressed. By using an extended state space vector, we introduce an integrator into the force control subsystem which results in a causal model. Thus we have shown that the basic ideas in the previous subsections are applicable to more complicated systems.

6 Conclusion

This paper addressed dynamic force control in overconstrained dynamic systems with special emphasis on robot control and multiarm coordination. First, the formulation in previous approaches to force control was shown to suffer from acausality. The acausality arises because rigid body dynamics is used to model the robot system. Two possible remedies are

suggested in the paper: (a) explicitly incorporating the actuator and contact dynamics into the dynamic equations; (b) introducing integrators in the control law. It is shown that the first remedy is appropriate when the sampling rate is much higher than or comparable to the characteristic frequency of the actuator dynamics, while the second is well suited to the case in which the characteristic frequency is much higher than the sampling frequency. Experimental results and computer simulations are presented to demonstrate the basic concepts and design guidelines are presented for force control algorithms. Finally, we illustrated the application of these ideas to more complex systems which require simultaneous force and position control. In particular we demonstrated a control scheme for controlling contact conditions in a multiarm manipulation system using computer simulation.

References

[1] A. Cole, J. Hauser, and S. Sastry. Kinematics and control of multifingered hands with rolling contact. In *Proceedings of 1988 International Conference on Robotics and Automation*, pages 228–233, Philadelphia, PA, April 1988.

[2] E. Colgate and N. Hogan. The interaction of robots with passive environments: applications to force feedback control. In *Advanced Robotics 1989, Proceedings of the Fourth International Conference on International Robotics*, pages 465–474, Columbus, Ohio, June 1989.

[3] S.D. Eppinger and W.P. Seering. On Dynamic Models of Robot Force Control. In *Proceedings of the IEEE International Conference on Robotics and Automation*, pages 29–34, April 1986.

[4] S.D. Eppinger and W.P. Seering. Three Dynamic Problems in Robot Force Control. In *Proceedings of the IEEE International Conference on Robotics and Automation*, pages 392–397, 1989.

[5] S.D. Eppinger and W.P. Seering. Understanding Bandwidth Limitations in Robot Force Control. In *Proceedings of the IEEE International Conference on Robotics and Automation*, pages 904–909, April 1987.

[6] N. Hogan. Impedance control: an approach to manipulation: part I. *Transactions of ASME, Journal of Dyamic Systems, Measurement, and Control*, 107(1):1–7, March 1985.

[7] H. Inoue. Computer controlled bilateral manipulator. *Bulletin, Japan Soc. Mech. Eng.*, 1971.

[8] A. Isidori. *Nonlinear Control Systems: An Introduction.* Springer-Verlag, Berlin, New York, 1985.

[9] H. Kazerooni. On the robot compliant motion control. *Transactions of ASME, Journal of Dynamic Systems, Measurement, and Control*, 111(3), September 1989.

[10] J. Kerr and B. Roth. Analysis of multifingered hands. *Int. J. of Robotics Research*, 4(4), 1986.

[11] O. Khatib. A unified approach for motion and force control of robot manipulator: the operational space formulation. *Journal of Robotics and Automation*, RA-3(1):43–53, February 1987.

[12] Antti J. Koivo and George A. Bekey. Report of workshop on coordinated multiple robot manipulators: planning, control, and application. *IEEE Journal of Robotics and Automation*, 4(1):91–93, February 1988.

[13] V. Kumar and K.J. Waldron. Force distribution in closed kinematic chains. *IEEE Journal of Robotics and Automation*, 4(6), December 1988.

[14] V. Kumar, X. Yun, E. Paljug, and N. Sarkar. Control of contact conditions for manipulation with multiple robotic systems. In *Proceedings of the IEEE International Conference on Robotics and Automation*, May 1991.

[15] L.Cai and A. A. Goldenberg. An approach to force and position control of robot manipulators. In *Proceedings of 1990 International Conference on Robotics and Automation*, pages 86–91, Cincinnati, OH, May 1990.

[16] Z. Li and S. Sastry. Task oriented optimal grasping by multifingered robot hands. *IEEE Transactions of Robotics and Automation*, 4(1), February 1988.

[17] N.H. McClamroch. Singular systems of differential equations as dynamic models for constrained dynamic systems. In *1986 IEEE International Conference on Robotics and Automation*, San Francisco, CA., April 1986.

[18] J.K. Mills and A.A. Goldenberg. Force and position control of manipulators. *IEEE Transactions on Robotics and Automation*, 5(1), February 1989.

[19] Eric Paljug, Xiaoping Yun, and Vijay Kumar. Control of rolling contacts in multiple robotic manipulation. In *Proceedings of the International Conference on Advanced Robotics*, pages 591–596, Pisa, Italy, 1991.

[20] Richard P. Paul. *Robot Manipulators: Mathematics, Programming, and Control.* The MIT Press, 1981.

[21] R.P. Paul and B. Shimano. Compliance and control. In *Proceedings of the JACC*, pages 694–699, 1976.

[22] George Pfreundschih, Vijay Kumar, and Tom Sugar. Design and control of a 3 dof in-parallel actuated manipulator. In *Proceedings of the IEEE International Conference on Robotics and Automation*, pages 1659–1665, Sacramento, California, 1991.

[23] Mark E. Pittelkau. Adaptive load-sharing force control for two-arm manipulators. In *Proceedings of 1988 International Conference on Robotics and Automation*, pages 498–503, Philadelphia, PA, April 1988.

[24] M. H. Raibert and J. J. Craig. Hybrid position/force control of manipulators. *Transactions of ASME, Journal of Dynamic Systems, Measurement, and Control*, 103(2):126–133, June 1981.

[25] J.K. Salisbury. Active stiffness control of a manipulator in cartesian coordinates. In *Proceedings of the 19th IEEE Conference on Decision and Control*, December 1980.

[26] K. Salisbury and B. Roth. Kinematics and force analysis of articulate mechanical hands. *ASME Journal of Mechanisms, Transmissions and Automation in Design*, 105:35–41, March 1983.

[27] S.A. Schneider and R.H. Cannon. Object impedance control for cooperative manipulation. In *Proceedings of the IEEE International Conference on Robotics and Automation*, Scottsdale, AZ, May 1989.

[28] Tom Sugar. *Modelling and Control of Pneumatic Actuators for Robots.* Master's thesis, University of Pennsylvania, 1991. In preparation.

[29] J. Wen and K. Kreutz. Motion and force control for multiple cooperative manipulators. In *Proceedings of the IEEE International Conference on Robotics and Automation*, Scottsdale, AZ, May 1989.

[30] Y. Xu and R.P. Paul. On position compensation and force control stability of a robot with a compliant wrist. In *IEEE International Conference on Robotics and Automation*, page , Philadelphia, PA, April 1988.

[31] B. Yi, R. Freeman, and D. Tesar. Open-loop stiffness control of overconstrained mechanisms/robotic linkage systems. In *Proceedings of the IEEE International Conference on Robotics and Automation*, Scottsdale, AZ, May 1989.

[32] T. Yoshikawa and K. Nagai. Evaluation and determination of the grasping forces in a multifingered grasp. In *Proceedings of 1988 International Conference on Robotics and Automation*, pages 245–248, Philadelphia, Pa, April 1988.

[33] T. Yoshikawa and X.Zheng. Coordinated dynamic hybrid control for multiple robots handling one constrained object. In *Proceedings of 1990 International Conference on Robotics and Automation*, Cincinnati, OH, May 1990.

[34] X. Yun. Coordination of two-arm pushing. In *Proceedings of the IEEE International Conference on Robotics and Automation*, pages 182–187, Sacramento, CA, April 1991.

[35] X. Yun and V. Kumar. An approach to simultaneous control of trajectory and interaction forces in dual arm configurations. In *Fourth International Conference on Advanced Robotics*, Columbus, Ohio, June 1989.

[36] X. Yun, V. Kumar, and N. Sarkar. Control of multiple arm systems with nonholonomic constraints. In *Submitted to the Proceedings of the IEEE International Conference on Robotics and Automation*, May 1992.

[37] Y. Zheng and J.Y.S. Luh. Optimal load distribution for two industrial robots handling a single object. In *IEEE International Conference on Robotics and Automation*, Philadelphia, PA, April 1988.

A Appendix: Description of the Experimental System

The single-degree-of-freedom pneumatic system consists of three major components, the valve/actuator mechanism, the computer and the amplifier.

The valve/actuator system was designed with off-shelf-components. Graphite glass actuators (Airpot) are used in order to minimize friction. Since only single-acting graphite-glass actuators are commercially available, and double acting action is desired, two actuators acting in opposite directions are used.

A flow control valve, Atchley 204, is used to control the flow of air. This valve adjusts the flow of air for a given voltage (If a zero voltage is commanded, the flow of air is stopped). The spool type valve consists of a flapper whose position is adjusted by a torque motor. The torque motor is controlled by an amplifier, which converts a signal of plus or minus ten volts to plus or minus ten milliamperes of current. The amplifier board also has an analog feedback loop which is needed for pressure feedback. Without pressure feedback, the static force-voltage calibration curve is very steep thus making force control virtually impossible. Pressure feedback is accomplished by two pressure transducers, SenSym 1620A, which are mounted at the inlet to the actuators. With the feedback, the force-voltage curve is flatter and quite linear. The valve to actuator distance is minimized by mounting the valve close to the actuators. This reduces the intermediate volume of air which in turn minimizes delays in the transmission line. and improves the performance of the system.

The force feedback is accomplished by a force sensor purchased from Zebra Robotics, Inc. The force sensor has six strain gauges and outputs six digital signals. The strain gauge readings are decoupled using a calibration matrix.

Data acquisition is done with an AT-computer using a data acquisition board and a digital input/output board. The digital I/O board is used to read the six strain gauge signals. The data acquisition board is used to send a voltage signal to the amplifier which controls the valve. The control program is written in C.